Electronic Supplementary Material (ESI) for Journal of Materials Chemistry A.

Hierarchical Platinum-Nickel@Platinum-Tin Core@Shell Nanowires Achieve Efficient Fuel Cell Catalysis

Liyuan Wang[a], Changhong Zhan[a], Wei Yan[a], Yunhua Li[a,*] and Lingzheng Bu[b,*]

a. State Key Laboratory of Physical Chemistry of Solid Surfaces, College of Chemistry and Chemical Engineering, Xiamen University, Xiamen, 361005, China.

b. College of Energy, Xiamen University, Xiamen, 361102, China.

Experimental Procedures

1.1 Chemicals.

Platinum (II) acetylacetonate ($Pt(acac)_2$, 97%) was purchased from Sigma-Aldrich. Nickel (II) acetylacetonate ($Ni(acac)_2$, 95%) and oleylamine (OAm, 80−90%) were supplied by Aladdin. Glucose (analytical reagent), dodecyl trimethyl ammonium chloride (DTAC, analytical reagent, 98%), tin (Ⅳ) chloride tetrahydrate ($SnCl_4{\cdot}4H_2O$, analytical reagent, 98%), methanol (analytical reagent, ≥ 99.5%), ethanol (analytical reagent, ≥ 99.7%), ethylene glycol (analytical reagent, ≥ 99.5%), cyclohexane (analytical reagent, ≥ 99.7%), and isopropanol (analytical reagent, ≥ 99.7%) were all purchased from Sinopharm Chemical Reagent Co., Ltd. (Shanghai, China). $HClO_4$ (analytical reagent, 70−72%) was purchased from Tianjin Zhengcheng Chemical Products Co. Ltd. Johnson Matthey 20 wt% Pt/C and Johnson Matthey 40 wt% Pt/C were purchased from Shanghai Hesen Electric Co., Ltd. 40 wt% PtRu/C was purchased from Suzhou Sinero Technology Co., Ltd. All the chemicals were used as received without further purification. All aqueous solutions were prepared using deionized water with a resistivity of 18.2 $M\Omega\ cm^{-1}$.

1.2 Materials synthesis.

In a typical synthesis of H-PtNi@PtSn NWs, 9.8 mg $Pt(acac)_2$, 2.3 mg $Ni(acac)_2$, 27.0 mg DTAC, 20.0 mg glucose and 5 mL OAm were added into a glass vial. After the mixture was ultrasonicated for around 1 h, it was then heated from room temperature to 180 °C and maintained for 30 minutes in an oil bath. And then the resulting homogeneous mixed solution was soaked in an oil bath and allowed naturally cool. After cooling to 80 °C, 4.4 mg $SnCl_4{\cdot}4H_2O$ dissolved in 1 mL OAm was then added dropwise to the above mixture under magnetic stirring. The reaction was then heated from 80 °C to 180 °C and kept for 5 h. The products were collected by centrifugation and washed three times with an ethanol/cyclohexane mixture. The synthesis conditions for H-PtNi@PtSn-l NWs, H-PtNi@PtSn-h NWs were similar to those of H-PtNi@PtSn NWs except changing the amount of $SnCl_4{\cdot}4H_2O$ to 2.2 mg and 6.6 mg, respectively. The Pt_3Ni NWs were synthesized via the similar formula to ultrathin PtNi NWs template used to form H-PtNi@PtSn NWs. The resulting homogeneous mixed solution was soaked in an oil bath of 180 °C for 5 h and allowed naturally cool. In a typical synthesis of PtSn NPs, 9.8 mg $Pt(acac)_2$, 4.4 mg $SnCl_4{\cdot}4H_2O$, 20.0 mg glucose and 5 mL OAm were added into a glass vial, and the resulting homogeneous mixed solution was soaked in an oil bath of 180 °C for 5 h and allowed naturally cool.

1.3 Characterization.

TEM was operated on JEM-1400 TEM at an accelerating voltage of 100 kV. HRTEM was conducted on a FEI Tecnai F30 TEM at an accelerating voltage of 300 kV. XRD measurement was conducted on an

Ultima-IV powder diffractometer equipped with a Cu radiation source (λ = 0.15406 nm). SEM-EDS was observed through ZEISS Sigma 300 field emission scanning electron microscope. The concentrations of the catalysts were determined by ICP-OES (ICAP 7000, ThermoFisher, USA). The X-ray photoelectron spectroscopy spectra were collected by XPS (Thermo Scientific, ESCALAB 250 XI). The carbon peak at 284.6 eV was used as the reference to correct for charging effects.

1.4 Electrochemical measurements.

The electrochemical measurements for MOR were performed on a threeelectrode system controlled by a CHI 660E electrochemistry workstation. The glassy-carbon electrode (GCE, diameter: 5 mm, area: 0.196 cm^2), graphite rod and saturated calomel electrode (SCE) were used as working electrode, counter electrode and reference electrode (the SCE was calibrated), respectively. Before test, GCE was polished with 0.3 and 0.05 mm Al_2O_3 slurry and then sonicated in ethanol and water each for several times. For the preparation of the electrode materials, the catalyst (3.0 mg) was mixed with isopropanol (1.0 mL) and Nafion solution (5.0 μL). The mixture was ultrasonicated for about 0.5 h to generate a homogeneous ink. After that, the working electrode was fabricated by casting 5 μL catalyst ink onto a GCE and then dried at room temperature. The electrolyte was 0.1 M $HClO_4$. The CVs were performed at room temperature in 0.1 M $HClO_4$ solution with the sweep rate of 50 mV s^{-1} and the potential range from –0.25 V to 0.96 V vs. SCE. A SCE was used as the reference electrode and converted to the RHE reference scale by Nernst equation. The MOR measurements were conducted in 0.1 M $HClO_4$ and 0.5 M CH_3OH solutions. The accelerated durability tests were carried out in 0.1 M $HClO_4$ between −0.1 V and 0.4 V vs. RHE at a scan rate of 100 mV s^{-1} for 1000 cycles. The accelerated durability tests were carried out in 0.1 M $HClO_4$ and 0.5 M CH_3OH solutions at 0.8 V vs. RHE. For the CO-stripping measurements, CO (99.99%) was bubbled at an open circuit for 30 min through 0.1 M $HClO_4$ solution in which the electrode immersed. The electrode was quickly moved to a fresh 0.1 M $HClO_4$ solution, and two cycles were recorded with a scan rate of 20 mV s^{-1}.

1.5 MEA performance tests.

Fuel cell experiments with a 1 × 1 cm^2 geometric area in a single cell were performed with the fuel cell test system. The typical anode catalytic layers of the MEA were prepared with 40% commercial Pt/C or H-PtNi@PtSn NWs/C. Catalyst inks for H-PtNi@PtSn NWs/C electrodes were prepared by mixing 10 mg of catalyst, 24 mg of a 5 wt % Nafion solution, and with 10 ml of aqueous ethanol. After an ice-bath ultrasonication for about 30 min, ink was applied on the carbon paper electrodes by spray-coating to obtain an active area of 1 × 1 cm^2. The prepared carbon paper electrodes as working electrodes were used in CV measurements to obtain H-PtNi@PtSn NWs/C electrodes. The MEA structures were obtained by the hot-pressing process at 120 °C for 180 s at 75 kg/cm^2 and the anode and cathode electrodes onto

the two sides of the Nafion 115 membrane (DuPont). For single-fuel cell tests at 80 °C, the flow rates of the methanol solution (5 M) and oxygen gas were fed at 1.0 mL/min and 100 sccm, respectively. The steady-state polarization curves were obtained after activating MEAs for at least 4 h.

1.6 Electrochemical measurements.

The electrochemical measurements for MOR were performed on a threeelectrode system controlled by a CHI 660E electrochemistry workstation. The glassy-carbon electrode (GCE, diameter: 5 mm, area: 0.196 cm^2), graphite rod and saturated calomel ele

1.7 Electrochemical in-situ FTIR spectroscopy.

Electrochemical *in-situ* FTIR spectroscopic experiments were conducted on a Nexus 870 FTIR (Nicolet) which is equipped with a liquid-nitrogen-cooled MCT-A detector, an EverGlo IR source and at a spectral resolution of 8 cm^{-1}. And infrared radiation sequentially passed through a CaF_2 window and a thin-layer solution (about 10 μm), and then it was reflected by the electrode surface. And the final resulting spectra were reported as a relative change which were defined as the following equation:

$$\frac{\Delta R}{R} = \frac{R(E_S) - R(E_R)}{R(E_R)}$$

$R(E_S)$ and $R(E_R)$ are the single-beam spectra collected at sample potential E_S and the reference potential E_R, respectively.

Supporting Figures

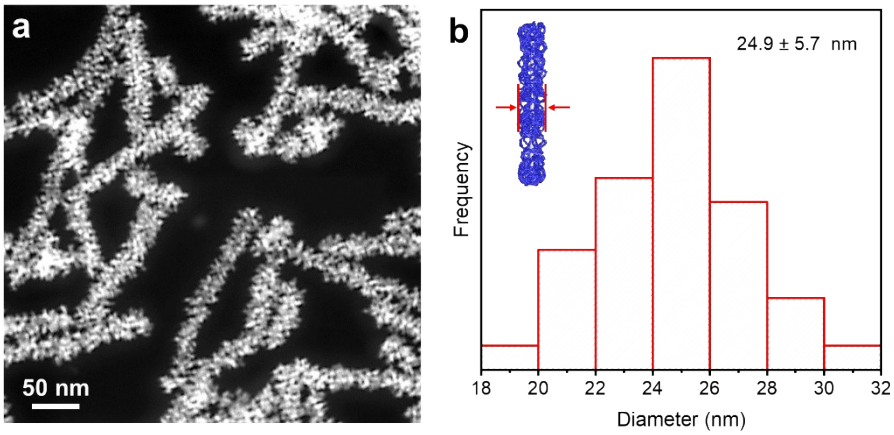

Figure S1. (**a**) HAADF-STEM image and (**b**) diameter distribution of H-PtNi@PtSn NWs.

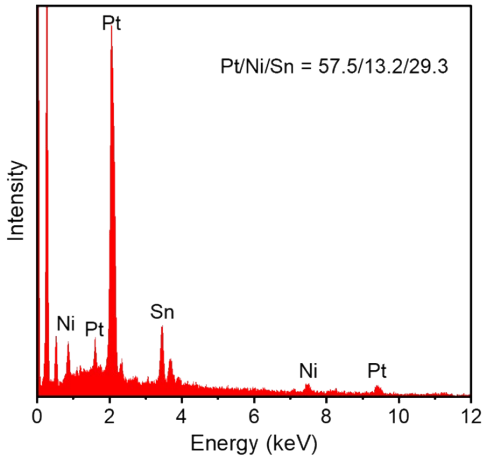

Figure S2. SEM-EDS of H-PtNi@PtSn NWs.

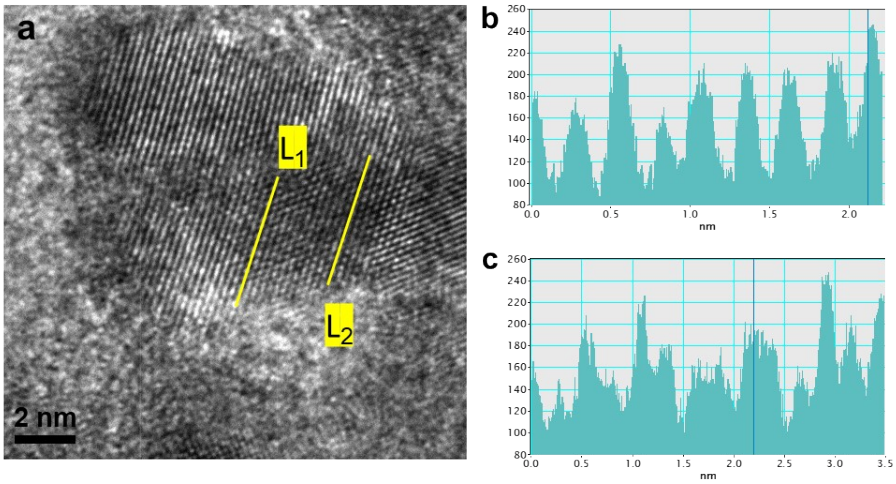

Figure S3. (**a**) HRTEM image of H-PtNi@PtSn NWs. (**b, c**) The intensity line profiles taken along the yellow lines (L_1 and L_2) in (**a**), respectively.

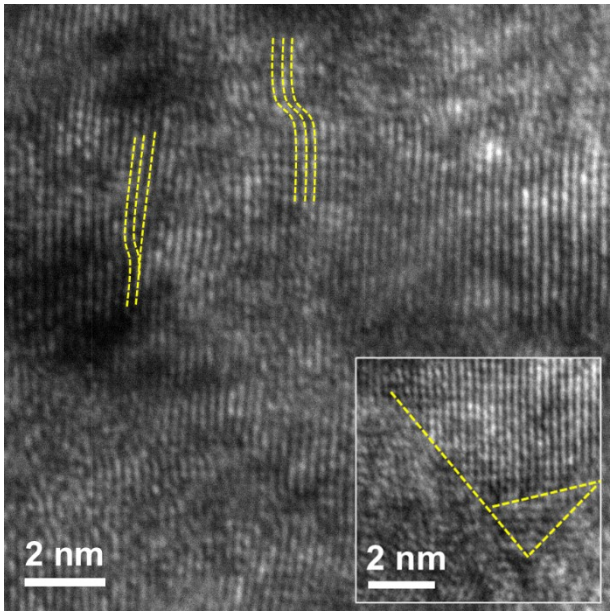

Figure S4. HRTEM image of H-PtNi@PtSn NWs. The inset is the HRTEM image of another region.

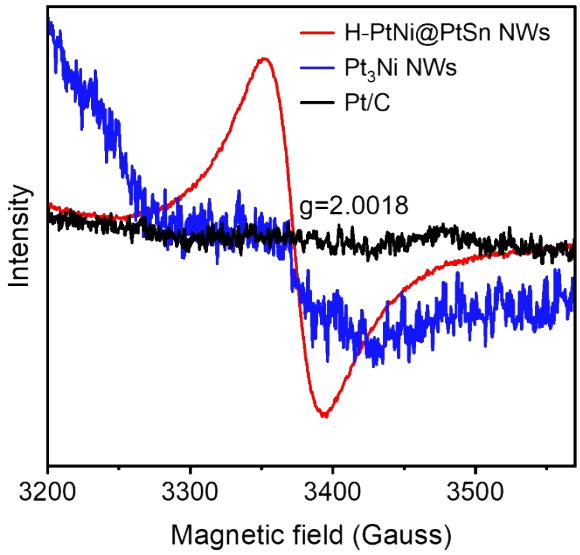

Figure S5. EPR spectra characterization for H-PtNi@PtSn NWs, Pt_3Ni NWs and commercial Pt/C.

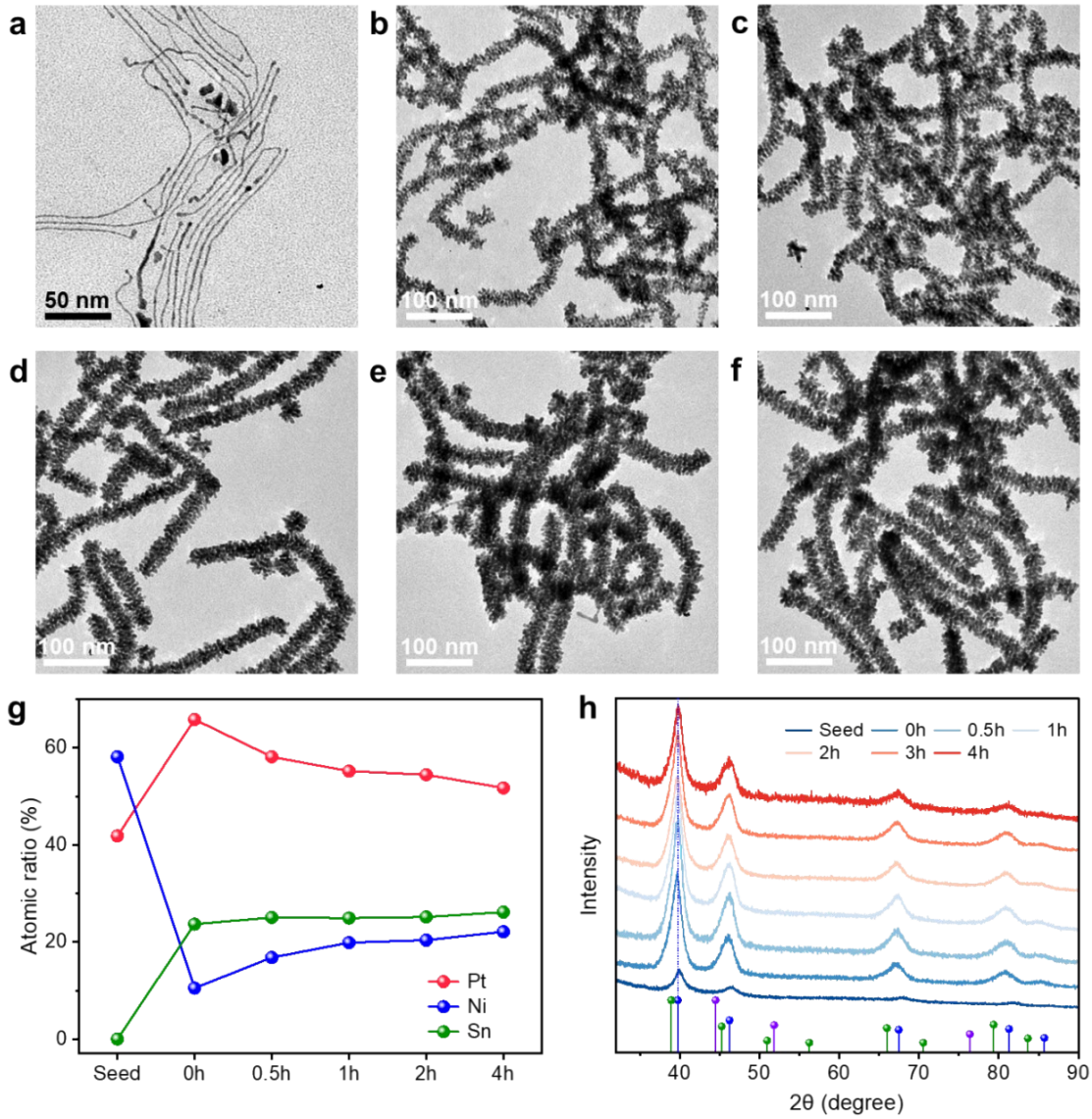

Figure S6. TEM images of H-PtNi@PtSn NWs intermediates obtained after the reaction proceeding for (**a**) 0.5 h, (**b**) reheating to 180 °C for 0 h, (**c**) 0.5 h, (**d**) 1 h, (**e**) 2 h, and (**f**) 4 h. (**g**) Atomic ratio changes of Pt, Ni, and Sn in different intermediates, as determined by SEM-EDS. (**h**) XRD patterns of these above intermediates.

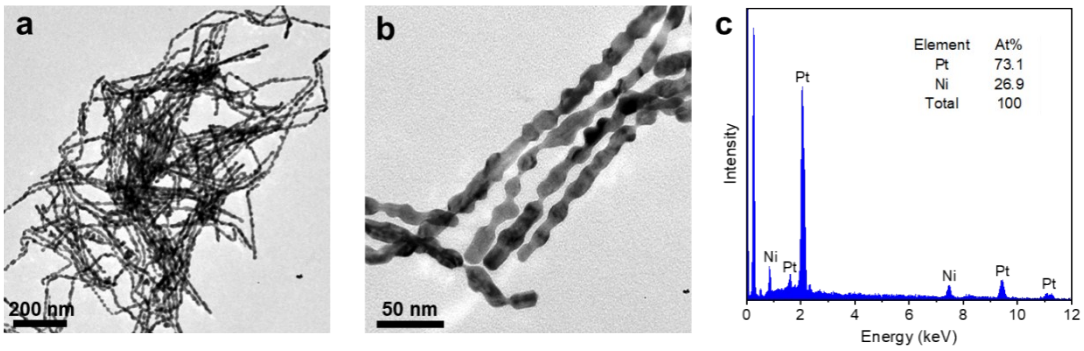

Figure S7. (**a, b**) TEM images and (**c**) SEM-EDS of Pt_3Ni NWs.

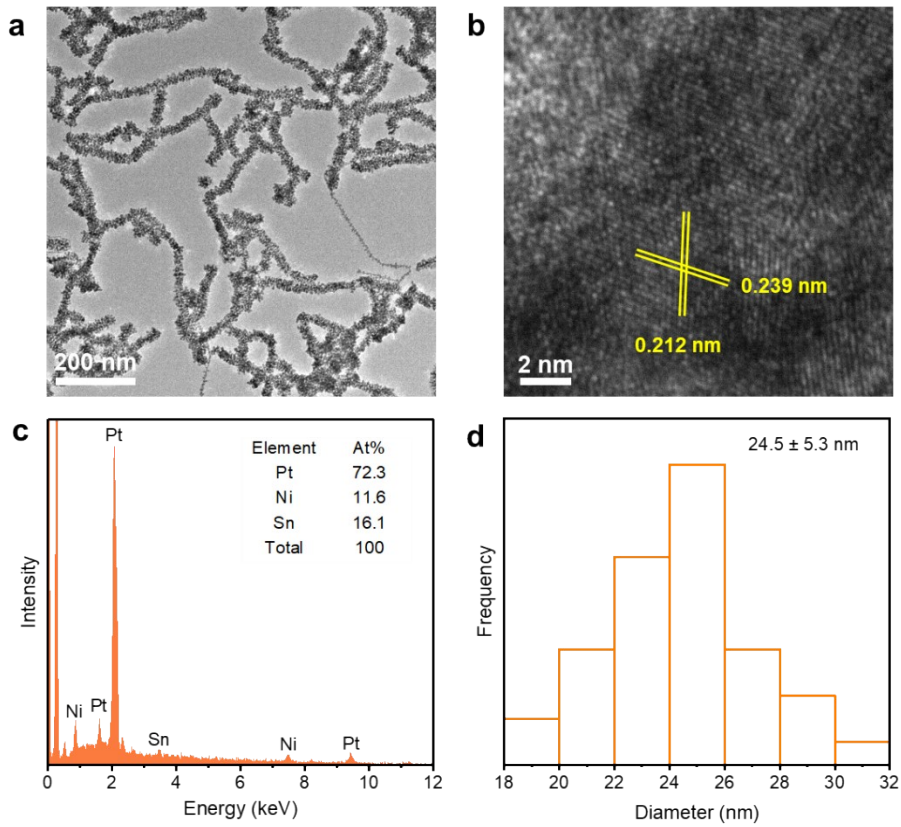

Figure S8. (**a**) TEM image, (**b**) HRTEM image, (**c**) SEM-EDS and (**d**) diameter distribution of H-PtNi@PtSn-l NWs.

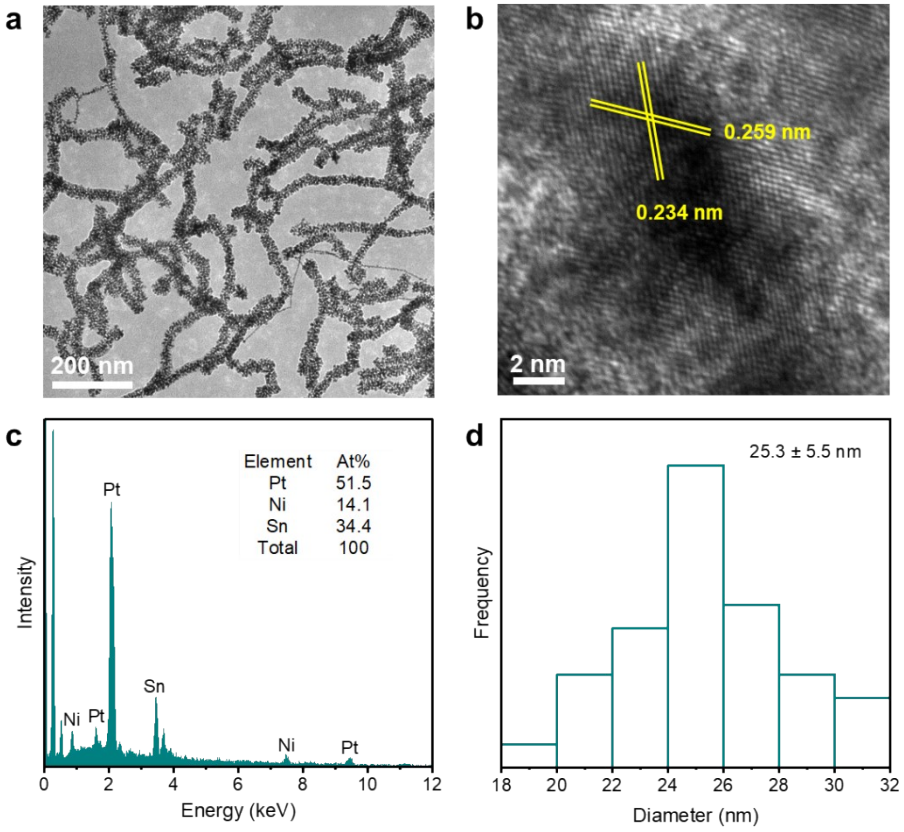

Figure S9. (**a**) TEM image, (**b**) HRTEM image, (**c**) SEM-EDS and (**d**) diameter distribution of H-PtNi@PtSn-h NWs.

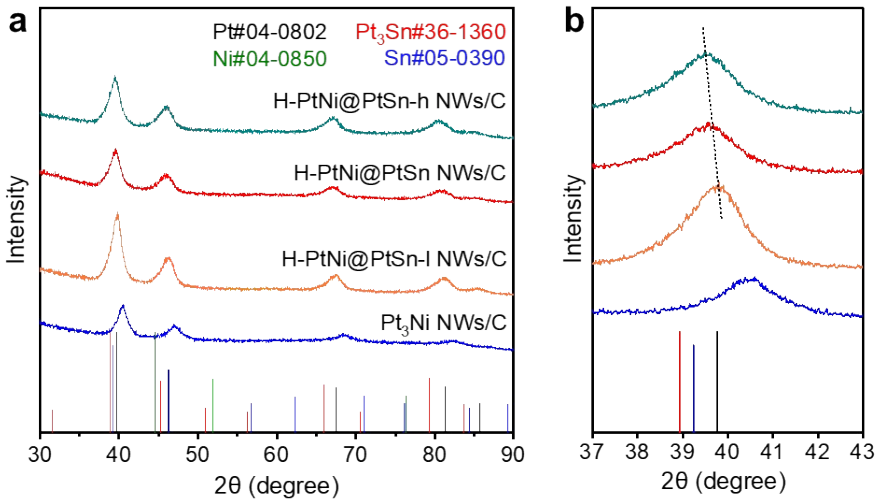

Figure S10. (**a**) XRD patterns and (**b**) enlarged XRD patterns of H-PtNi@PtSn-l NWs/C, H-PtNi@PtSn NWs/C, H-PtNi@PtSn-h NWs/C and Pt_3Ni NWs/C.

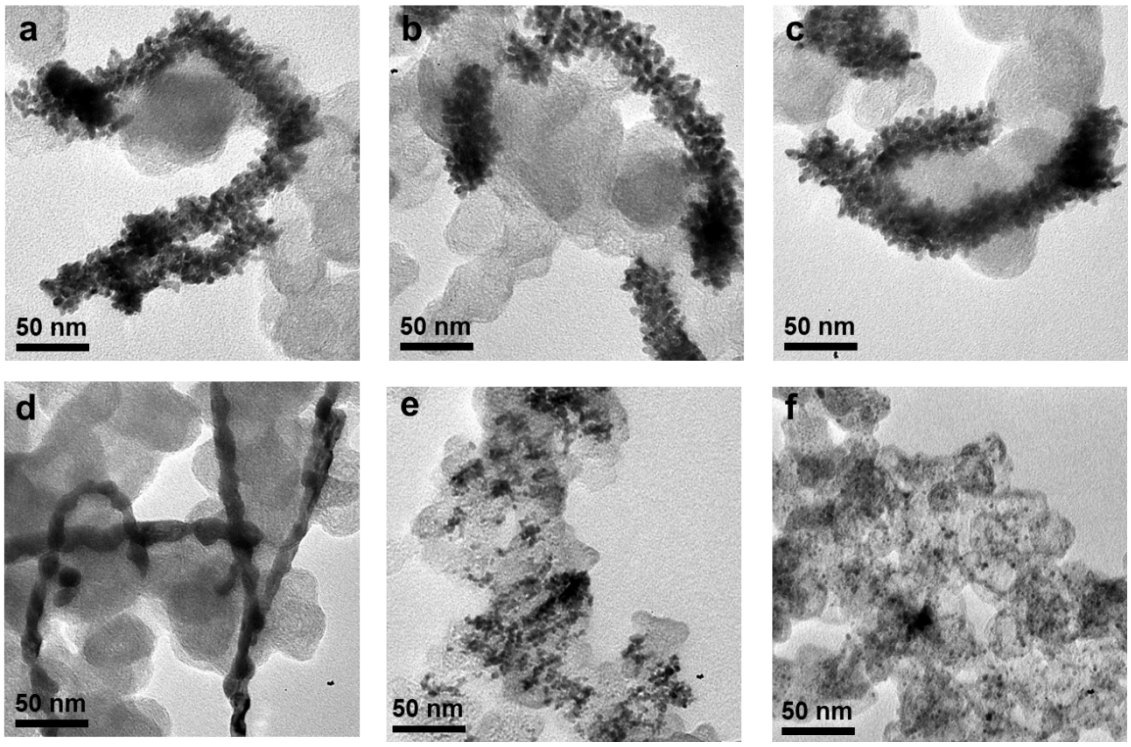

Figure S11. TEM images of (**a**) H-PtNi@PtSn-l NWs/C, (**b**) H-PtNi@PtSn NWs/C, (**c**) H-PtNi@PtSn-h NWs/C, and (**d**) Pt_3Ni NWs/C, (**e**) commercial PtRu/C and (**f**) commercial Pt/C.

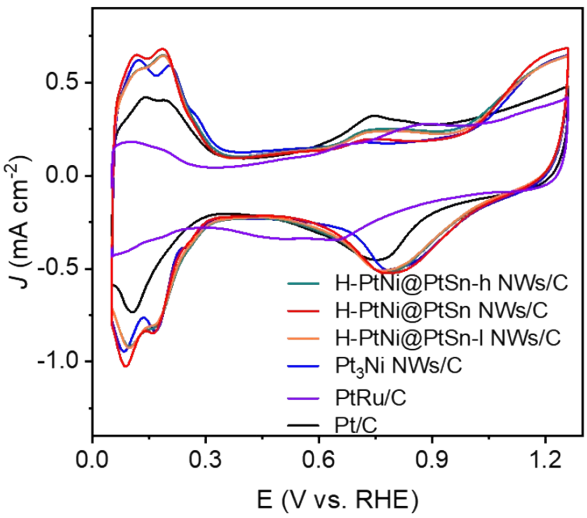

Figure S12. CV curves of different catalysts in 0.1 M $HClO_4$.

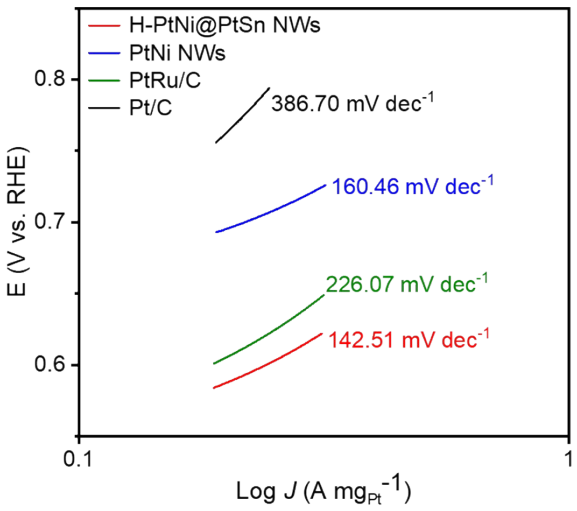

Figure S13. Tafel plots of different catalysts for MOR.

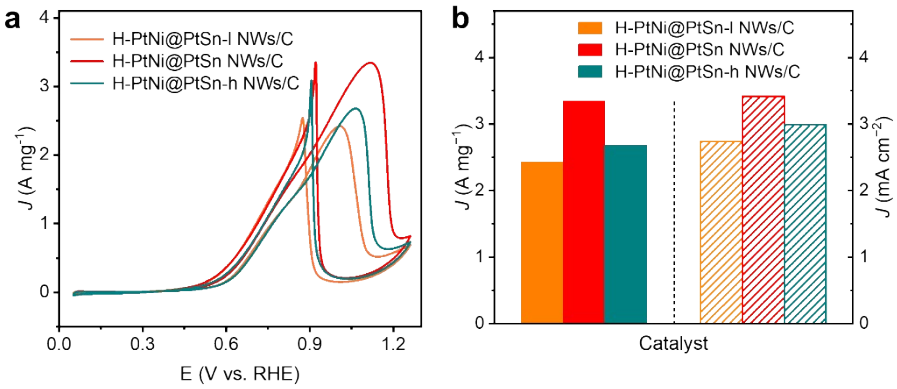

Figure S14. (**a**) CV curves and (**b**) histograms of specific and mass activities for different catalysts toward MOR measured in 0.1 M $HClO_4$ + 0.5 M methanol at a scan rate of 50 mV s^{-1}.

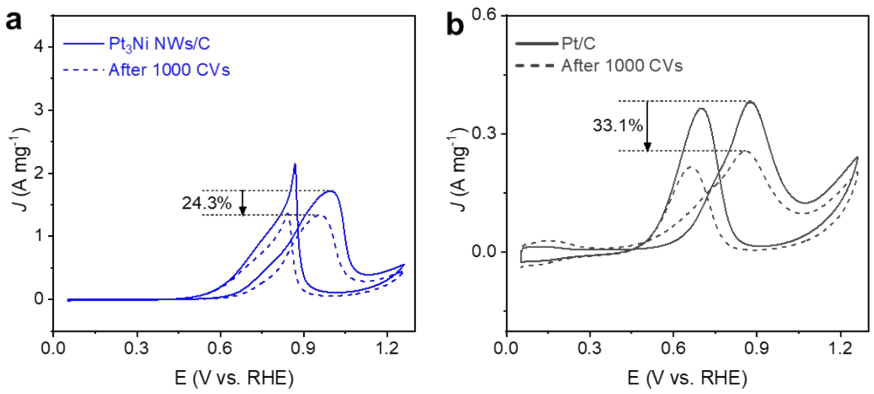

Figure S15. The changes of MOR mass activities for (**a**) Pt_3Ni NWs/C and (**b**) commercial Pt/C before and after 1000 CV cycles.

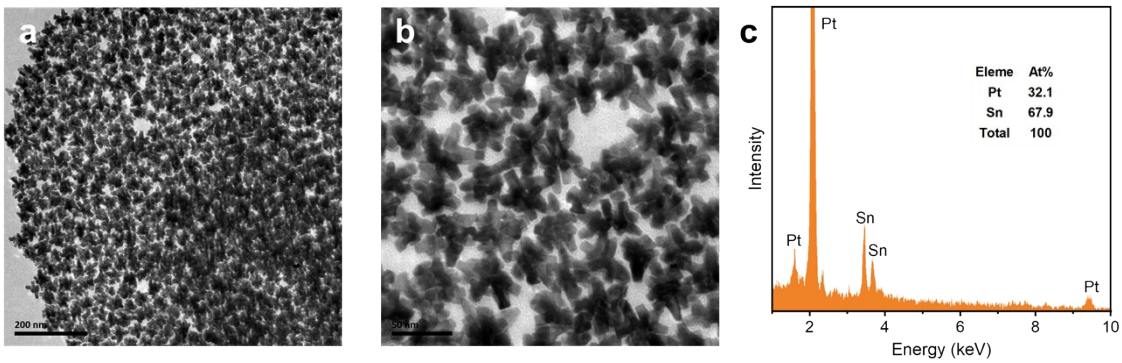

Figure S16. (**a, b**) TEM images and (**c**) SEM-EDS of PtSn NPs.

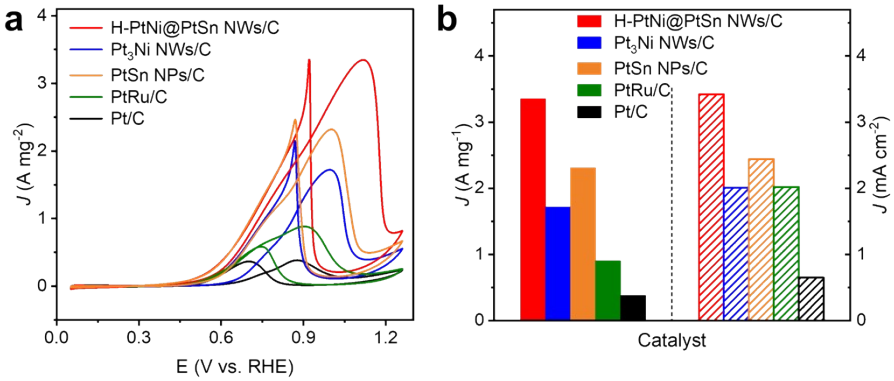

Figure S17. (**a**) CV curves of different catalysts measured in 0.5 M methanol + 0.1 M $HClO_4$ solution. (**b**) Specific and mass activities of different catalysts.

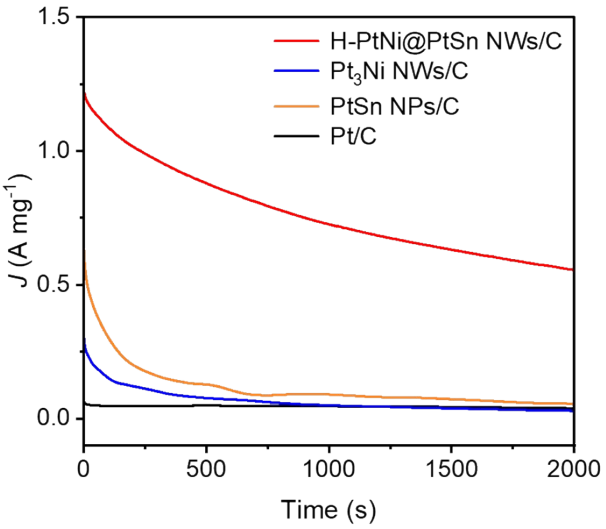

Figure S18. I-t measurements for H-PtNi@PtSn NWs/C, Pt_3Ni NWs/C, PtSn NPs/C and commercial Pt/C recorded at 0.8 V vs. RHE for 2000 s.

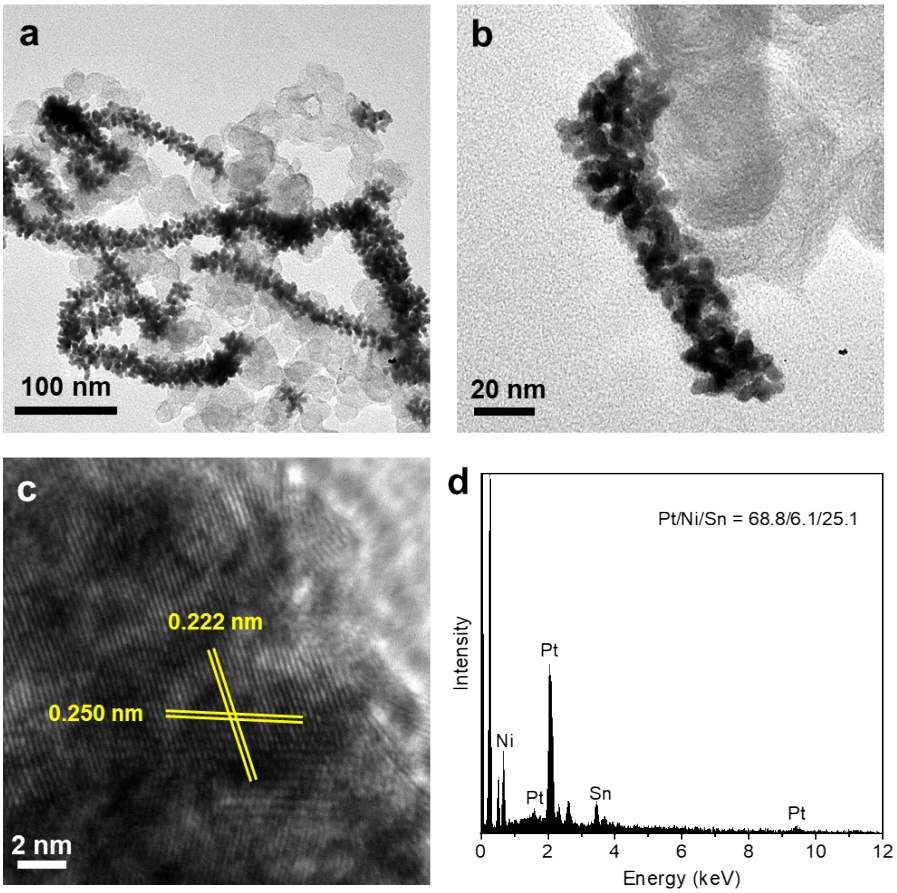

Figure S19. (**a, b**) TEM images, (**c**) HRTEM image and (**d**) SEM-EDS of H-PtNi@PtSn NWs/C after the i-t test for 2000 s.

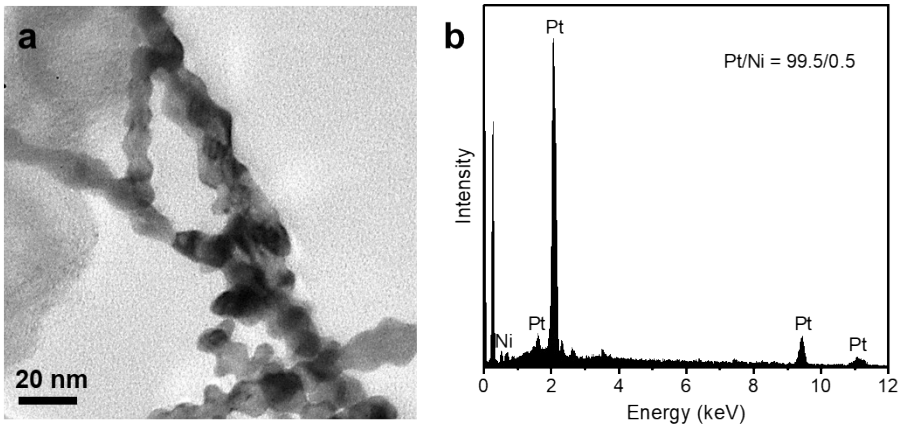

Figure S20. (**a**) TEM image and (**b**) SEM-EDS of Pt_3Ni NWs/C after the i-t test for 2000 s.

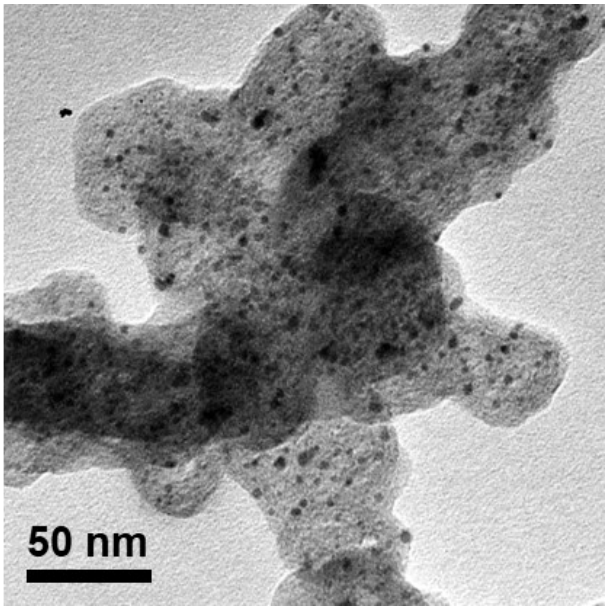

Figure S21. TEM image of commercial Pt/C after the i-t test for 2000 s.

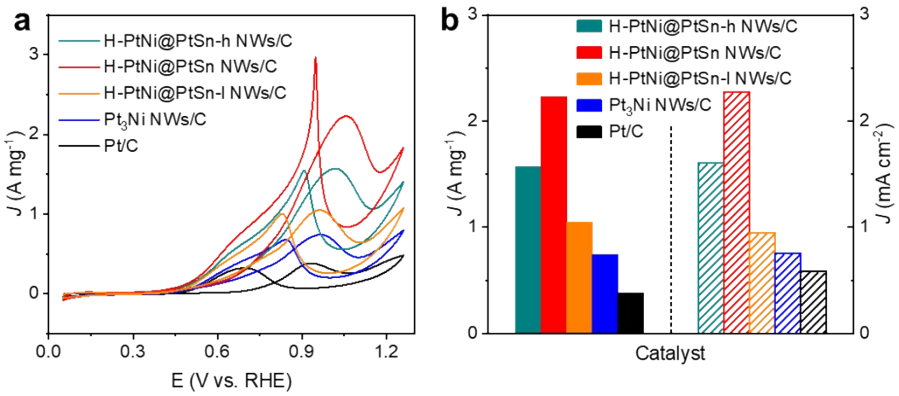

Figure S22. (**a**) CV curves and (**b**) histograms of specific and mass activities for different catalysts toward EOR measured in 0.1 M $HClO_4$ + 0.5 M ethanol at a scan rate of 50 mV s^{-1}.

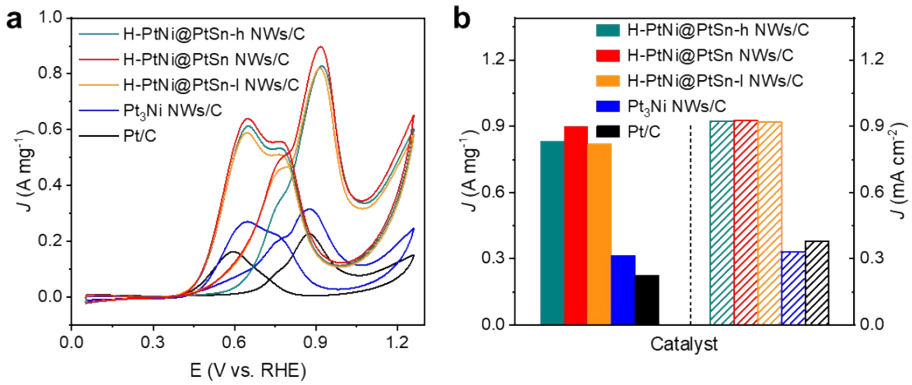

Figure S23. (**a**) CV curves and (**b**) histograms of specific and mass activities for different catalysts toward EGOR measured in 0.1 M $HClO_4$ + 0.5 M ethylene glycol at a scan rate of 50 mV s^{-1}.

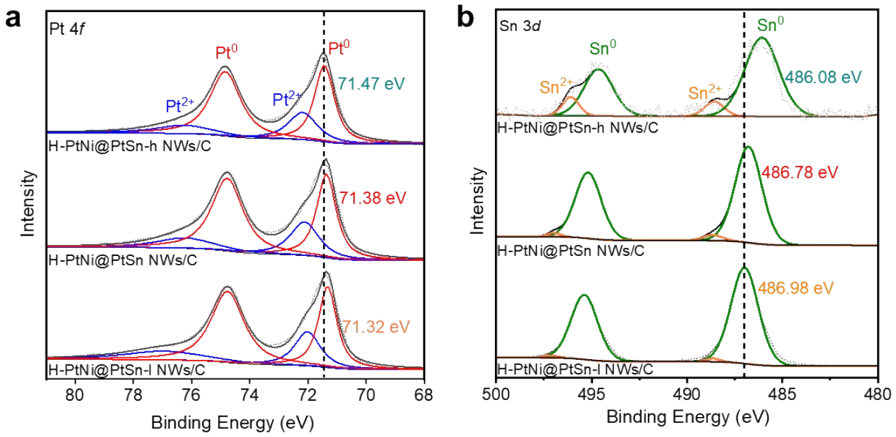

Figure S24. (**a**) Pt 4*f* and (**b**) Sn 3*d* XPS spectra of H-PtNi@PtSn-l NWs/C, H-PtNi@PtSn NWs/C and H-PtNi@PtSn-h NWs/C.

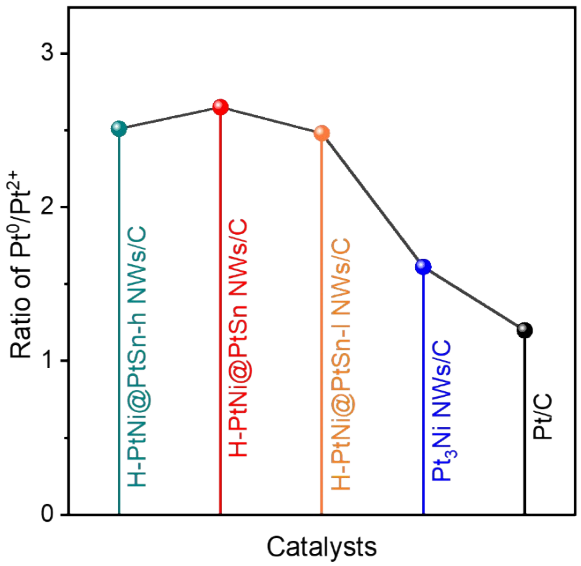

Figure S25. Ratios of Pt^0/Pt^{2+} for different catalysts.

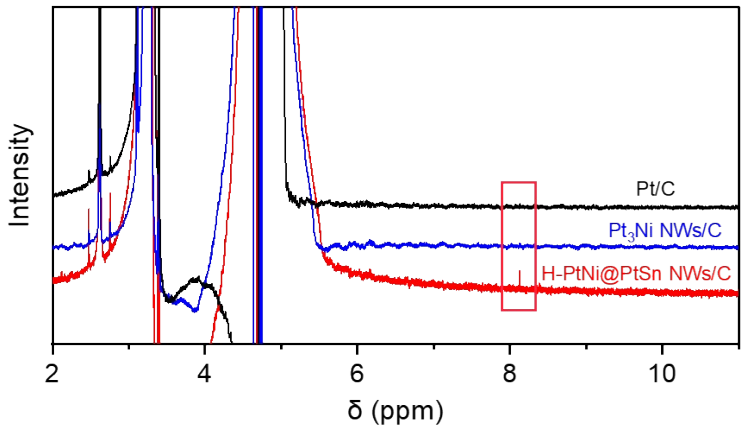

Figure S26. ^{1}H-NMR spectra of the electrolytes obtained after the running i-t tests on H-PtNi@PtSn NWs/C, Pt_3Ni NWs/C and commercial Pt/C.

Supporting Tables

Table S1. Atomic ratios of Pt/Ni/Sn for H-PtNi@PtSn-l NWs, H-PtNi@PtSn NWs, H-PtNi@PtSn-h NWs, Pt_3Ni NWs and PtSn NPs/C obtained from SEM-EDS and ICP-OES.

Sample	Atomic ratios of Pt/Ni/Sn or Pt/Ni (Sn) (%)	
	SEM-EDS	ICP-OES
H-PtNi@PtSn-l NWs	72.3/11.6/16.1 (1/0.16/0.22)	75.3/9.9/14.8 (1/0.13/0.20)
H-PtNi@PtSn NWs	57.5/13.2/29.3 (1/0.23/0.51)	59.8/11.6/28.6 (1/0.19/0.48)
H-PtNi@PtSn-h NWs	51.5/14.1/34.4 (1/0.27/0.67)	53.4/13.6/33.0 (1/0.25/0.62)
Pt_3Ni NWs	74.8/25.2 (1/0.33)	77.6/22.4 (1/0.29)
PtSn NPs/C	67.9/32.1 (1/0.47)	65.6/34.4 (1/0.52)

Table S2. MOR performance comparison for H-PtNi@PtSn-l NWs/C, H-PtNi@PtSn NWs/C, H-PtNi@PtSn-h NWs/C, Pt_3Ni NWs/C, PtSn NPs/C, commercial PtRu/C and commercial Pt/C.

Catalyst	ECSA	Mass activity	Specific activity
	($m^2\ g^{-1}$)	($A\ mg^{-1}_{Pt}$)	($mA\ cm^{-2}$)
H-PtNi@PtSn-l NWs/C	88.64	2.43	2.74
H-PtNi@PtSn NWs/C	**97.95**	**3.35**	**3.42**
H-PtNi@PtSn-h NWs/C	89.53	2.68	2.99
Pt_3Ni NWs/C	85.51	1.72	2.01
PtSn NPs/C	94.67	2.31	2.44
PtRu/C	44.50	0.90	2.02
Pt/C	58.88	0.38	0.65

Table S3. MOR performance comparison for H-PtNi@PtSn NWs/C and other reported Pt-based catalysts.

Catalyst	Electrolyte	Mass activity ($A\ mg_{PGM}^{-1}$)	Specific activity ($mA\ cm^{-2}$)	Durability (Mass activity)	Ref.
H-PtNi@PtSn NWs/C	**0.1 M $HClO_4$ + 0.5 M CH_3OH**	**3.35**	**3.42**	**54.9% after 2000 s and 79.4% after 1000 cycles**	**This work**
d-Pt_2Cu_1 NWs	0.1 M $HClO_4$ + 0.5 M CH_3OH	2.23	5.27	4.67% after 3600 s	[1]
22% YO_x/MoO_x-Pt	0.1 M $HClO_4$ + 0.5 M CH_3OH	2.10	3.35	64.7% after 1200 cycles	[2]
H-PtSSs/C	0.1 M $HClO_4$ + 0.5 M CH_3OH	2.89	/	77% after 3600 s	[3]
h-PtNiCo/C	0.1 M $HClO_4$ + 0.5 M CH_3OH	2.82	5.73	37.5% after 3600 s	[4]
$Pt_{0.68}Cu_{0.18}Ru_{0.14}$ NFs	0.1 M $HClO_4$ + 0.5 M CH_3OH	0.81516	7.65	17.6% after 5000 s	[5]
CeOx/ PtCu/CeCuOx/C	0.5 M H_2SO_4 + 0.5 M CH_3OH	0.3325	0.92	95.3% after 600 cycles	[6]
A-PNTs	0.5 M H_2SO_4 + 1 M CH_3OH	2.56	5.37	/	[7]
PtNiRh NWs	0.1 M $HClO_4$ + 0.5 M CH_3OH	1.72	2.49	/	[8]
P-PtNi CNC	0.5 M H_2SO_4 + 2 M CH_3OH	0.38	3.85	/	[9]
Pt_{CF3}NPs/C	0.1 M $HClO_4$ + 0.5 M CH_3OH	0.56	16.8	/	[10]

Table S4. MEA performance comparison for H-PtNi@PtSn NWs/C and other reported Pt-based catalysts.

Catalyst	Methanol concentration	Temperature	Power density	Stability	Ref.
			($mW\ cm^{-2}$)	(Activity retention %)	
H-PtNi@PtSn NWs/C	**5 M**	**80 ℃**	**65.1**	**82.6 %, 20 h, at 0.4 V**	**This work**
PtCu NWs	1 M	80 ℃	49.7	~94%, 24 h, at 50 $mA\ cm^{-2}$	[1]
Pt-$NiTiO_3$/C	1 M	80 ℃	32.8	~78%, 5 h, at 100 $mA\ cm^{-2}$	[11]
ASP Pt NWs	1 M	75 ℃	63.9	/	[12]
PtRu/C-20% IrO_2	2 M	60 ℃	22	/	[13]
PtRuMo/CNTs	2 M	60 ℃	61.3	/	[14]

Table S5. Deconvoluted XPS peak positions (unit: eV) for H-PtNi@PtSn-l NWs/C, H-PtNi@PtSn NWs/C, H-PtNi@PtSn-h NWs/C, Pt_3Ni NWs/C and commercial Pt/C, including Sn^0 $2p_{5/2}$, Ni^0 $2p_{3/2}$ and Pt^0 $4f_{7/2}$.

Sample	Deconvoluted XPS peak position (unit: eV)		
	Pt^0 $4f_{7/2}$	Ni^0 $2p_{3/2}$	Sn^0 $3d_{5/2}$
H-PtNi@PtSn-l NWs/C	71.32	852.57	487.01
H-PtNi@PtSn NWs/C	71.38	852.62	486.79
H-PtNi@PtSn-h NWs/C	71.47	852.67	486.09
Pt_3Ni NWs/C	71.20	852.51	/
Pt/C	71.89	/	/

References

1. K. Wang, D. Huang, Y. Guan, F. Liu, J. He, Y. Ding, *ACS Catal.* 2021, **11**, 14428–14438.
2. M. Li, Z. Zhao, W. Zhang, M. Luo, L. Tao, Y. Sun, Z. Xia, Y. Chao, K. Yin, Q. Zhang, L. Gu, W. Yang, Y. Yu, G. Lu, S. Guo, *Adv. Mater.* 2021, **33**, e2103762.
3. Y. Feng, Z. Zhao, F. Li, L. Bu, Q. Shao, L. Li, J. Wu, X. Zhu, G. Lu, X. Huang, *Nano Lett.* 2021, **21**, 5075–5082.
4. H. Ma, Z. Zheng, H. Zhao, C. Shen, H. Chen, H. Li, Z. Cao, Q. Kuang, H. Lin, Z. Xie, *J. Mater. Chem. A* 2021, **9**, 23444–23450.
5. M. Qiao, F. Y. Meng, H. Wu, Y. Wei, X. F. Zeng, J. X. Wang, *Small* 2022, **18**, e2204720.
6. Y. Wang, Z. Li, X. Zheng, R. Wu, J. Song, Y. Chen, X. Cao, Y. Wang, Y. Nie, *Appl. Catal. B Environ.* 2023, **325**, 122383.
7. F. Xu, S. Cai, B. Lin, L. Yang, H. Le, S. Mu, *Small* 2022, **18**, e2107387.
8. W. Zhang, Y. Yang, B. Huang, F. Lv, K. Wang, N. Li, M. Luo, Y. Chao, Y. Li, Y. Sun, Z. Xu, Y. Qin, W. Yang, J. Zhou, Y. Du, D. Su, S. Guo, *Adv. Mater.* 2019, **31**, e1805833.
9. A. Fan, C. Qin, R. Zhao, H. Sun, H. Sun, X. Dai, J.-Y. Ye, S.-G. Sun, Y. Lu, X. Zhang, *Nano Res.* 2022, **15**, 6961–6968.
10. Q. Lenne, A. Mattiuzzi, I. Jabin, L. Troian-Gautier, J. Hamon, Y. R. Leroux, C. Lagrost, *ChemSusChem* 2023, **16**, e202201990
11. T. Kumaresan, T. Velumani, M. Chandran, K. Palaniswamy, A. Thirkell, A. Fly, R. Chen, S. Sundaram, *Mater. Lett.* 2020, **276**, 128222.
12. K. Lin, Y. Lu, S. Du, X. Li, H. Dong, *Inter. J. Hydrogen Energy* 2016, **41**, 7622–7630.
13. V. Baglio, D. Sebastián, C. D'Urso, A. Stassi, R. S. Amin, K. M. El-Khatib, A. S. Aricò, *Electrochim. Acta* 2014, **128**, 304–310.
14. S. Chen, F. Ye, W. Lin, *Inter. J. Hydrogen Energy* 2010, **35**, 8225–8233.